Effect of cast part size on the microstructure and mechanical properties of a bainitic High-Carbon and High-Silicon Cast Steel

N. E. Tenaglia
Advanced Steel Processing and Products Research Center, Colorado School of Mines 1500 Illinois St, Golden, CO 80401, USA
ntenaglia@mines.edu, http://orcid.org/0000-0001-6372-88816372-8881

D. O. Fernandino, A. D. Basso
INTEMA, Universidad Nacional de Mar del Plata-CONICET, Av. Colón 10850, Mar del Plata, B7606BVZ, Argentina
dfernandino@fi.mdp.edu.ar, https://orcid.org/0000-0003-4647-2663
abasso@fi.mdp.edu.ar, https://orcid.org/0000-0002-6167-4426

Citation: Tenaglia, N. E., Fernandino, D. O., Basso, A. D., Effect of cast part size on the microstructure and mechanical properties of a bainitic High-Carbon and High-Silicon Cast Steel, Fracture and Structural Integrity, 71 (2025) 80-90.

Received: 31.07.2024
Accepted: 04.10.2024
Published: 12.10.2024
Issue: 01.2025

KEYWORDS. Cast part size, Microsegregation, Bainitic transformation, High-carbon high-silicon cast steel, Mechanical properties.

INTRODUCTION

In the last decades, there have been significant advances in the development of ultra-high-strength steels [1-7]. Particularly, an ultra-fine, carbide-free bainite (CFB) has been developed from high-carbon, high-silicon steels through austempering heat treatments [4-5]. These microstructures are composed of bainitic ferrite plates and retained austenite with film and blocky morphologies. The great interest in this steel family is due to the use of low proportions of inexpensive alloying elements, the simple processing route and the favorable combination of mechanical properties. The ultrafine thickness of bainitic ferrite promotes high strength and toughness, while the absence of carbides provides high resistance to cleavage fracture and void formation. Also, during plastic deformation, retained austenite may transform to martensite, increasing the strain-hardening rate, delaying the necking and thus enhancing the steel ductility by a transformation-induced plasticity (TRIP) effect [6-7]. In general, this generation of steels has showed tensile properties comparable with other more

expensive steels such as Maraging steels [8-9]. The literature reports CFB steels with remarkable combinations of ultimate tensile strength and total elongation (2.1 GPa and 21%, respectively) and of ultimate tensile strength and fracture toughness (2.5 GPa and 30 MPa m1/2) [7,8,10]. Moreover, remarkable fatigue [11] and wear performance [12] have also been reported. Investigations on the development of CFB steels have been mainly focused on steels previously homogenized and hot rolled or forged. This process minimizes solute segregation and refine the solidification structure, which causes a better performance of pieces due to a more homogeneous distribution of alloying elements. Nevertheless, many steel parts produced for the automotive, mining or oil industries are normally obtained through the melting and casting processes, such as crankshafts, camshafts, pump bodies, suspension parts, etc. [13]. It is widely known that the microstructure and mechanical properties of castings differ from those obtained by rolling or forging with the same chemical composition, mainly due to the presence of casting defects, for example, non-metallic inclusions, porosity, voids, micro-shrinkage and segregation (macro and/or micro) of alloying elements [14-19]. Microsegregation promotes a heterogeneous distribution of alloying elements at the microstructural scale. During steel solidification in sand moulds, microsegregation can be particularly significant, especially when the cast parts require further heat treatment to achieve the desired final microstructure [17-19]. Solid-state transformations are strongly influenced by chemical composition. Thus, a non-uniform distribution of alloying elements could lead to the formation of undesired phases after a specific heat treatment, degrading mechanical properties and in-service performance, such as wear resistance [20-21].

To commercialize cast components with CFB microstructures, it is necessary to characterize the heat treatment kinetics, the resulting bainitic microstructures and the associated mechanical properties. The authors of this work have developed studies in this area, particularly focusing on the segregation phenomena in high-silicon cast steels[15-19]. In Basso et al [17], the macro and microsegregation patterns of Cr, Mn, and Si in high-carbon high-silicon steel by using different 'Y' block sizes were investigated. The results of this contribution revealed that the partition coefficient of these elements is lower than unity (k<1), i.e., all these elements segregate into the interdendritic zones during the primary formation of austenite from the melt, resulting in a significant chemical heterogeneity. In all analyzed samples, the dendritic regions (First To Freeze zones, FTF) were clearly solute-lean, while interdendritic regions (Last To Freeze zones, LTF) were solute-enriched. In the case of the samples obtained from Y-block thickness of 12.5 mm, a higher microsegregation level compared to the samples obtained from Y-blocks thickness of 75 mm was measured. The self-back diffusion mechanism was assumed to be responsible for the lower level of microsegregation in the thicker casting. The high volume of steel causes a very slow cooling rate during solidification, promoting the diffusion of alloying elements and resulting in chemical homogenization.

To enhance the characterization of CFB cast steels, this study aims to investigate the influence of varying casting thicknesses on the progression of the bainitic transformation at different temperatures, as well as the mechanical properties of the resultant bainitic microstructures.

EXPERIMENTAL PROCEDURE

Material

The high-carbon and high-silicon cast steel (Fe-0.82C-2.20Si-1.05Mn-0.95Cr, wt.%) used in this study was produced in an industrial foundry using a medium-frequency induction furnace of 1500Kg capacity. Silica green sand was employed for the moulds. The chemical composition was selected based on prior studies about bainitic steels available in the literature. The C and Si contents were chosen to ensure bainite formation at low temperatures and to suppress cementite precipitation from the austenite during the transformation, respectively. Additionally, Cr and Mn were added to enhance the steel's hardenability [22]. The casting process involved pouring the melt into Y-block sand moulds (ASTM A897M) of two different thicknesses to investigate the influence of casting part size (solidification structure). The dimension 12.5 and 75 mm corresponds to the thickness of the Y-block legs, which is the usable part of the block (Fig. 1). The thicknesses of the Y-blocks studied were chosen based on the thicknesses of the cast parts that can be manufactured using this bainitic cast steels. Samples machined from the 25 mm Y-block are referred to as "thinner samples", while those machined from the 75 mm Y-block are referred to as "thicker samples".

Test samples

Several test samples were machined from the legs of the thinner and the thicker Y-blocks. For dilatometry testing, samples with a diameter of 4 mm and a length of 10 mm were prepared. To characterize the mechanical properties and conduct microstructural analysis, samples with a diameter of 15 mm and a length of 100 mm were initially pre-machined to facilitate the heat treatment processes. Then, the samples were further machined to produce subsize tensile specimens according to

ASTM E8 standards. The microstructural characterization was conducted on samples extracted from the pre-machined specimens after the heat treatment.

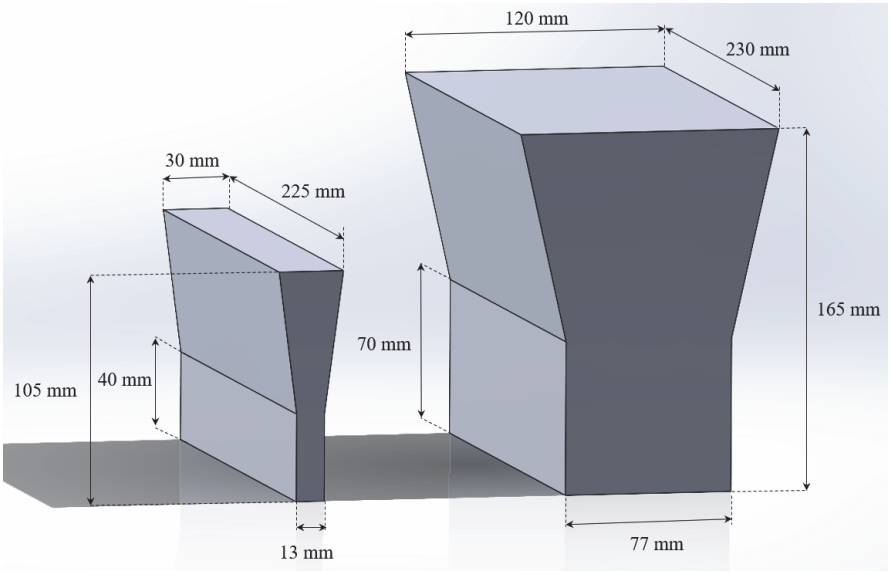

Figure 1: Scheme of `Y´ blocks used in the present work.

Heat treatments

The martensite starts temperature (Ms) determination and the evaluation of the bainitic reaction at different temperatures were performed by using a TA 805 DIL A/D dilatometer. A type S thermocouple spot-welded to the surface of the sample was used to monitor and control temperature. The samples were heated and held isothermally at the austenitizing temperature under vacuum. Helium was used during the cooling and austempering steps.

The thermal cycle used for the Ms determination consisted of a full austenitization step at 920°C for 60 min, followed by quenching down to room temperature at a cooling rate of 50 °C/s, which is sufficient to avoid high-temperature transformations during cooling. To estimate the Ms, the offset method proposed by Yang and Bhadeshia [23] was applied. This method defines the Ms as the point at which a specific strain, corresponding to the formation of 1 vol.% of martensite, is reached. In this work, an offset of 0.02% was adopted, close to the one suggested by Yang and Bhadeshia.

Once the Ms was determined, austempering heat treatments were designed. Since the Ms represents the lower temperature limit for the isothermal bainite formation, austempering temperatures of 230°C, 280°C and 330°C were selected. The thermal cycle used to obtain the desired microstructures involved full austenitization at 920 °C for 60 minutes, followed by quenching to the transformation temperature at a rate of 50 °C/s. The samples were held at different austempering temperatures for 360 minutes before cooling to room temperature.

The metallographic preparation and the microstructural observation of austempered samples were performed using standard methods, including a final polishing step with 1 μm diamond paste. The microstructures were revealed using Nital 2% etching. Micrographs were taken using light optical (LOM) and scanning electron microscopy (SEM) in a Nikon Epiphot 200 (Nikon Instruments, Inc., Melville, NY, USA) and a Zeiss Crossbeam 350 FEG-SEM microscope (operated at 15.0 kV), respectively. X-ray diffraction (XRD) measurements were carried out to quantify the retained austenite in the microstructures. The analysis was performed with a Panalytical X'pert Pro operated at 40 kV and 40 mA and using a Cu anode (with a characteristic wavelength $k\alpha = 1.542$ Å). The diffractometer is equipped with a graphite monochromator to filter the $k\beta$ radiation. Each sample was step scanned in the range of $2\theta = [38–86°]$ with a step size of 0.015. The retained austenite fraction was calculated from the integrated intensities of (200), (220), and (311) austenite peaks, and those of (002), (112), and (022) planes of ferrite, according to standard ASTM E975.

The samples for mechanical testing were austenitized at 920 °C for 60 minutes in a box furnace. After austenitization, the samples were quickly transferred to molten salt bath (50% sodium nitrite—50% potassium nitrate) set at the selected austempering temperatures and held for 360 minutes. The samples were then cooled down to room temperature in water.

Hardness measurements were performed using Vickers indentation under 5 kg load, following the ASTM E10 standard. The reported hardness values for each microstructure represent the average of five measurements. Tensile tests were conducted according to the ASTM E8 standard, using specimens of 6.35 mm diameter in an Instron testing machine.

RESULTS

Martensite start temperature

Fig. 2 shows characteristic dilation curves as relative change in length (RCL) as a function of temperature obtained during cooling at 50 °C/s from austenitization step. It can be observed that there is a difference in the Ms for the different casting thicknesses. The estimated Ms were 161±5 and 174±5 °C for the thicker and thinner cast samples respectively.

These results can be understood by considering the microsegregation process. It is well known that microsegregation profiles depend on cooling rate, partition coefficients (k), and secondary dendrite arm spacing. In a previous study [17], the authors examined in detail the influence of different casting sizes on macro- and microsegregation. The findings showed that samples obtained from thinner casting exhibited a higher degree of microsegregation. During solidification, Cr, Mn, and Si are rejected into the remaining liquid, as their k are less than 1. Consequently, LTF regions are enriched in solutes, while the FTF regions have the lowest solute concentrations. In this context, the relationship between the chemical composition of cast steel and the Ms can be assessed using Eqn. (1) [24], where different local Ms may be expected for the same steel due to microsegregation. The inhomogeneous distribution of alloying elements in the matrix affects the onset and progression of the martensitic transformation, altering the Ms [25,26]. Regions depleted of alloying elements will transform to martensite first, while segregated areas will transform later. Therefore, as segregation levels increase, the Ms is expected to increase. As a result, the thinner cast sample exhibits a higher Ms compared to the thicker sample.

$$\text{Ms (°C)} = 539 - 423\,(\%C) - 30.4\,(\%Mn) - 17.7\,(\%Ni) - 12.1\,(\%Cr) - 7.5\,(\%\,Mo, W, Si) \quad (1)$$

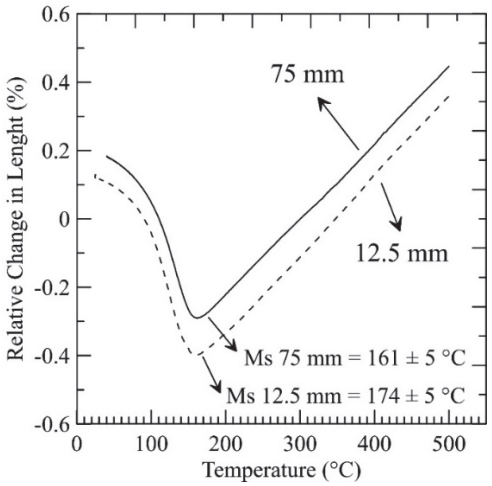

Figure 2: RCL as a function of temperature during cooling at 50 °C/s for the thinner and thicker cast samples (samples obtained from Y-block thicknesses of 12.5 mm and 75 mm respectively).

Austempering heat treatments

Figs. 3a and 3b shows the evolution of RCL and its derivate (DRCL), as a function of holding time for the three temperatures investigated (Fig. 3a corresponds to the thinner cast sample, while Fig. 3b is for the thicker casting). It is evident that the advance of the bainitic reaction with the holding time exhibits a characteristic sinusoidal pattern, as widely reported [27–28]. The formation of bainitic ferrite from austenite results in volume expansion (sample expansion) due to the differing atomic volumes of austenite and ferritic bainite. Therefore, these curves were only used to estimate the time at which the transformation stops, rather than determining phase fraction. The transformation time was determined within the stable region of the RCL, using the method based on the DRCL. A threshold of 4% of the maximum value of DRCL was chosen, following the approach of Santajuana et al [28], to identify the point at which the bainitic reaction stops.

From the analysis of Figs. 3a and 3b, it can be observed that the bainitic transformation rate rises as the austempering temperature increases. For the case of the thicker cast samples austempered at 280 and 330 °C, the transformation stop time is shorter compared to the thinner cast samples. This discrepancy could be attributed to the lower level of segregation shown by thicker Y-block. The bainitic transformation stops when the carbon content in the remaining austenite reaches the T0 curve, which depends on chemical composition. Higher segregation results in a broader T0 curve, i.e., the transformation will stop at different carbon contents in LTF and FTF areas. A steel with higher microsegregation requires

more time to stop the bainitic transformation due to the presence of LTF zones with higher solute content [15-18]. However, the time difference is not significant, suggesting that the segregation levels assessed may not significantly influence the transformation times. At 230°C, the transformation has not concluded after 360 minutes for either cast samples thickness. The transformation stops times determined for each condition is summarized in Tab. 1.

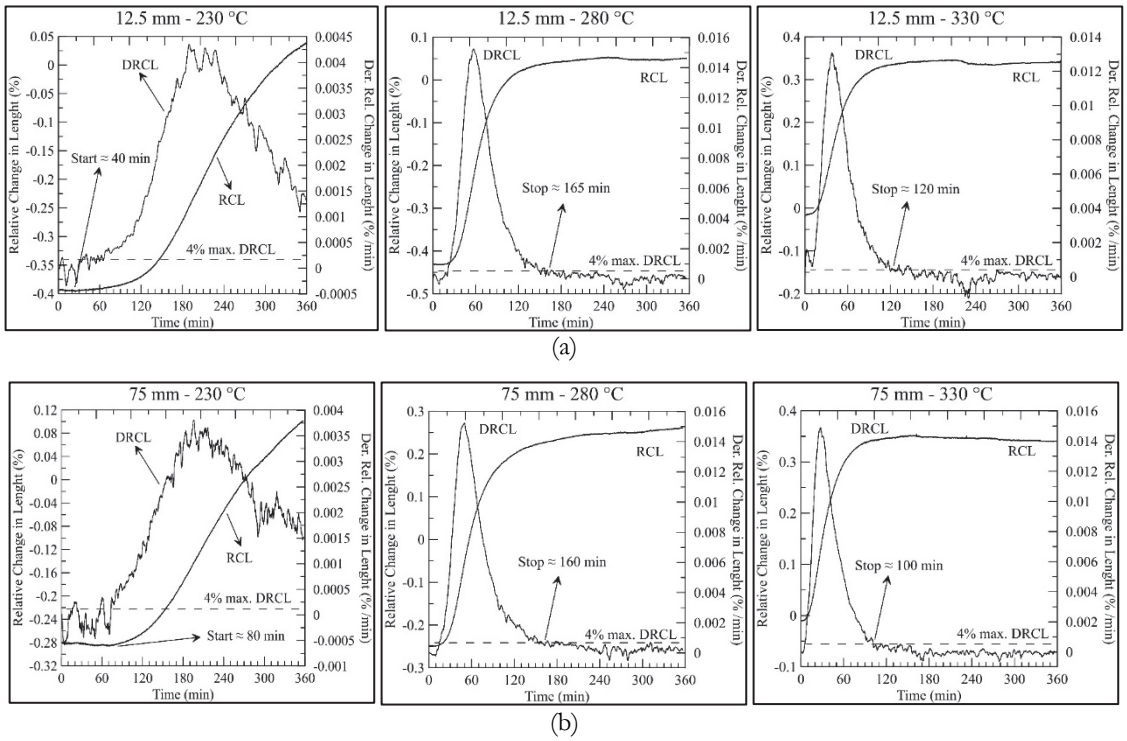

Figure 3: RCL and DRCL as a function of time during isothermal heat treatments at 230, 280 and 330 °C, for (a) thinner cast sample, (b) thicker cast sample. Transformation stop times were estimated by means of the DRCL.

Austempering Temperature (°C)	Cast sample thickness (mm)	Transformation time (min)
230	12.5	> 360
	75	> 360
280	12.5	165
	75	160
330	12.5	120
	75	100

Table 1: Transformation stop times determined by the DRCL method.

Microstructural characterization

Fig. 4 shows LOM images corresponding to samples austempered at 230°C for 360 minutes and subsequently quenched to room temperature. Fig. 4a, 4c and 4e correspond to thinner casting, while Fig. 4b, 4d and 4f, to the thicker cast samples. The low magnification used in Fig. 4a and 4b allows revealing differences in the microsegregation pattern. As expected, a coarser solidification structure is evident as the casting size increases (or the solidification rate decreases). Fig. 4c and 4d depict higher magnification micrographs revealing dendritic and interdendritic zones in both the thinner and thicker Y-block. The micrographs show that the bainitic transformation initiates in the FTF zones (darker regions in Fig. 3b), which contain lower level of substitutional solutes (Cr, Si and Mn) and exhibit the lowest hardenability. The LTF zones consist of martensite/austenite due to a lower level of transformation. Fig. 4e and 4f provide a detailed view of these microstructural features. The presence of fresh, non-tempered martensite significantly affects the ductility of steel. Fresh martensite is a hard and brittle phase, characterized by its tetragonal structure with a high concentration of carbon atoms, which induces internal stresses and increases brittleness. In this steel, it forms during the final cooling (quenching) due to the incomplete bainitic transformation. Consequently, the steel's ductility is drastically reduced, making it more susceptible to cracking under mechanical stress [29].

It is important to note the difference in the progress of the bainitic transformation between the thinner and thicker cast samples. Fig. 4 clearly shows a greater transformation degree in the thinner cast sample, relating to its levels of segregation. As previously mentioned, the samples from the thinner Y-block have higher levels of segregation, with FTF zones containing lower concentrations of alloying elements and LTF zones with higher concentrations. This promotes the bainitic transformation to initiate earlier in the FTF zones of these samples compared to the same zones in the thicker cast sample, which has less segregation. The difference in bainitic transformation start times was evident in the dilatometry tests (see Fig. 3), with the initiation time being approximately 40 minutes and 80 minutes for the thinner and thicker cast samples respectively (see Fig. 3a vs. Fig. 3b). Considering that bainitic ferrite plates act as nucleation sites for new plate nucleation (autocatalysis), the early formation of bainite in the thinner cast samples accelerated the overall transformation. These results confirm that the segregation present in the microstructure modifies the kinetics of bainitic transformation.

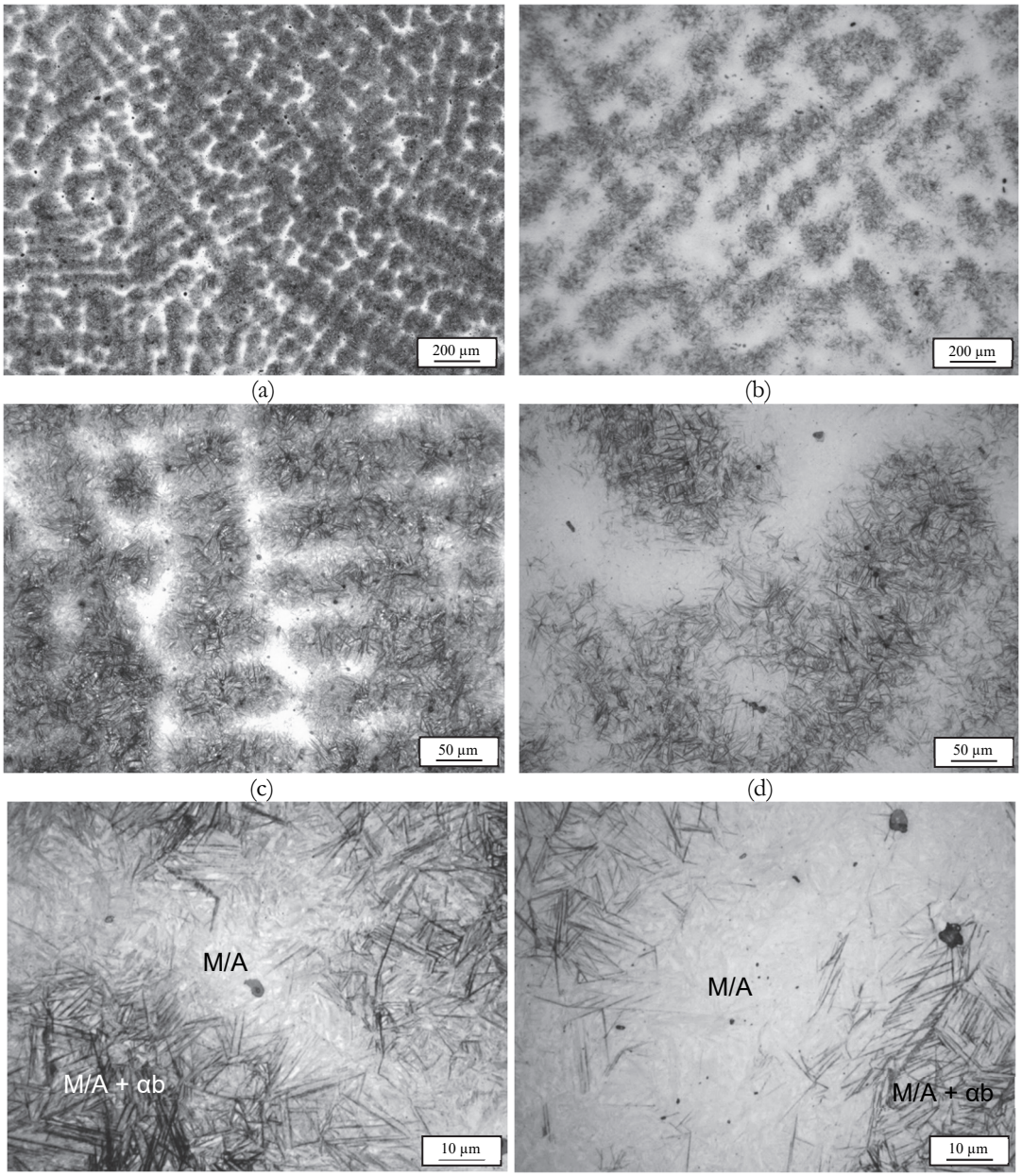

Figure 4: Micrographs corresponding to samples austempered at 230 °C for 360 min. (a), (c) and (e) thinner casting sample; (b), (d) and (f) thicker casting sample. Symbol αb stands for bainitic ferrite, M for martensite and A for retained austenite. LOM, Nital (2%).

Fig. 5 shows the microstructures obtained after austempering treatments at 280°C for 360 minutes. The microstructures are composed by bainitic ferrite with plate morphology and retained austenite (both as blocks and films). No martensite was

observed after extensive examination, suggesting that, if present, its amount is very low. Under these heat treatment conditions, the bainitic transformation stop has been achieved (see Fig. 3 or Tab. 1). Additionally, it can be observed that Nital 2% etching highlights differences in the solidification structure (compare Figs. 5a and 5b). However, no differences in the bainitic structure were found when observed by SEM (compare Figs. 5e vs 5f). It could be concluded that the segregation difference does not affect the quantity and morphology of phases present in the microstructure (bainitic ferrite and retained austenite) for treatment times longer than the stop of bainitic transformation. Both the FTF and LTF zones of the thinner and thicker casting samples showed a similar structure, although the distribution of LTF zones is finer in the thinner casting samples.

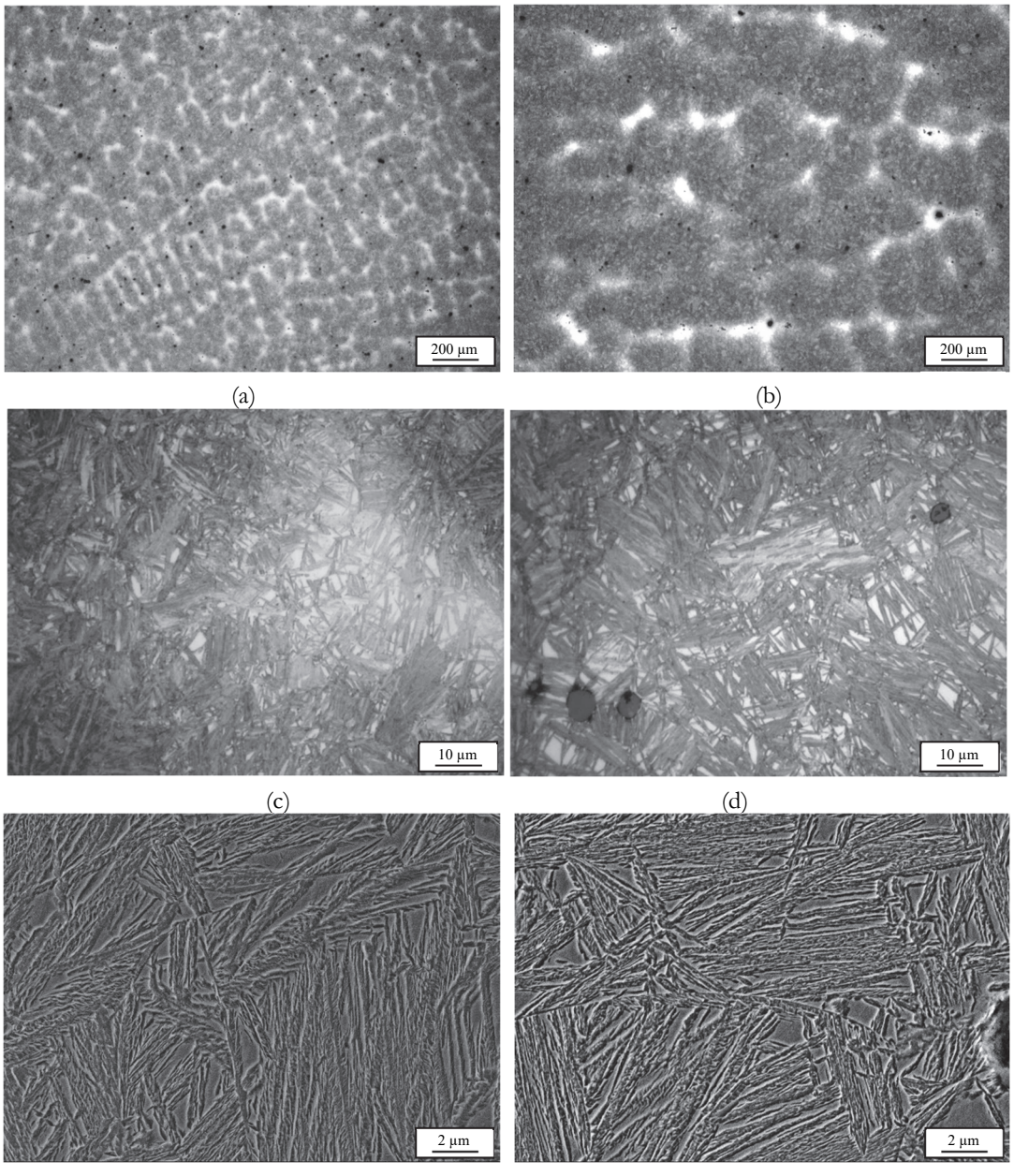

Figure 5: Micrographs corresponding to samples austempered at 280 °C for 360 minutes. (a), (c) and (e) thinner casting sample; (b), (d) and (f) thicker casting sample. LOM and SEM, Nital 2%.

Fig. 6 shows the microstructure obtained after austempering treatments at 330°C for 360 minutes. Again, microstructures are composed of bainitic ferrite and retained austenite, and no martensite was identified. Under these heat treatment conditions, the bainitic transformation is also complete. From the comparison to the Fig. 5, a thicker microstructure with larger bainitic ferrite plates and a higher amount of retained austenite is observed. Additionally, no significant differences

were found in the microstructures from the different cast samples thicknesses at high magnification. The influence of other factors, such as strain and dislocations, was not considered in the kinetics of the bainitic transformation. As mentioned, the steel in this study was produced by casting, avoiding subsequent plastic deformation processes like rolling or hot forging, which typically involve significant deformation and modify the dislocation density of the material.

The volume fraction of retained austenite, measured using XRD, and the hardness values for samples austempered at 230°C, 280°C, and 330°C for 360 minutes are shown in Tab. 2. These results are in good agreement with the microstructures showed in Figs. 4 to 6, and it can be explained as follows. The bainitic reaction starts with the formation of bainitic ferrite plates from austenite under paraequilibrium conditions, i.e., there is no diffusion of alloying elements. Immediately after the ferrite plates grow, carbon is partitioned from the bainitic ferrite to the surrounding austenite. The high silicon concentration prevents the carbide precipitation from the austenite, which is typically found in conventional bainite. As the reaction progresses, the carbon content in the remaining austenite increases until it reaches the T0 line; at this point, there is no driving force for further transformation of austenite into ferrite, stopping the bainitic transformation and resulting in a microstructure composed of bainitic ferrite and austenite [26]. As the austempering temperature decreases, the microstructure becomes more refined and contains a lower fraction of retained austenite. At lower austempering temperatures, the parent austenite is stronger, leading to the formation of thinner bainitic ferrite plates since these need to deform the austenite to grow. Additionally, at lower transformation temperatures, the precipitation of bainitic ferrite can further proceed before the austenite carbon concentration reaches the T0 line, resulting in a higher fraction of bainitic ferrite and, consequently, a lower proportion of retained austenite. Finally, due to the greater extent of the transformation, the blocks of retained austenite at lower temperatures are smaller.

The microstructural characteristics described can be observed in the SEM images in Figs. 5 and 6. As the austempering temperature increases, the bainitic ferrite becomes thicker and the retained austenite blocks become larger, resulting in overall coarser microstructures. Additionally, Tab. 2 shows that the amount of retained austenite increases with higher austempering temperatures, while hardness values decrease. It is important to note that no significant differences are observed in the retained austenite and hardness values between the different cast samples thicknesses. This confirms that besides the distribution of FTF and LTF areas, the microstructures obtained from different casting thicknesses for fixed austempering temperature and time are very similar.

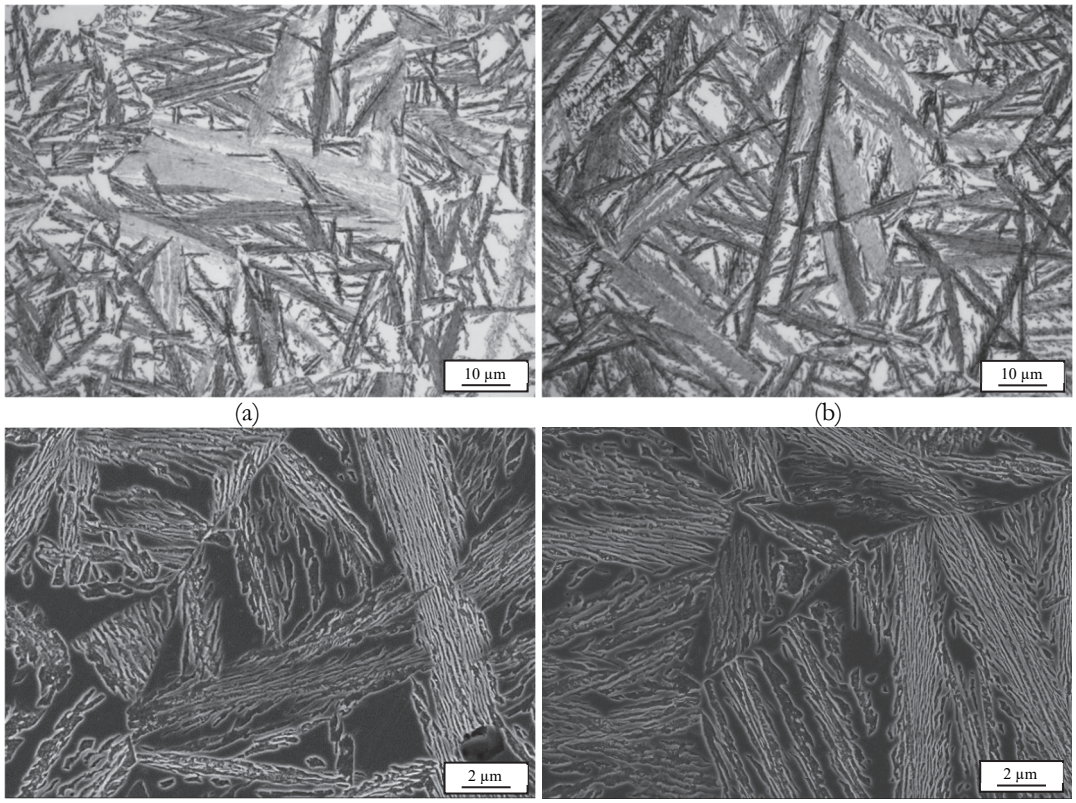

Figure 6: Micrographs corresponding to samples austempered at 330 °C for 360 minutes. (a), (c) thinner casting sample, (b), (d) thicker casting sample. LOM and SEM, Nital 2%.

Austempering Temperature (°C)	Cast sample thickness (mm)	Retained austenite content (%)	Hardness (HV5)
230	12.5	22±1	803±20
	75	19±1	807±20
280	12.5	27±1	598±15
	75	26±1	600±15
330	12.5	36±2	472±15
	75	38±2	467±15

Table 2: Volume fraction of retained austenite measured with XRD and hardness values for samples austempered at 230°C, 280°C and 330°C for 360 minutes.

Mechanical properties

Tab. 3 shows the ultimate tensile strength (UTS), yield strength (YS) and total elongation of samples austempered at 280°C y 330°C for both cast samples thickness evaluated. The result of UTS and YS are also plotted in Fig. 7. The mechanical properties corresponding to samples austempered at 230°C were not considered due to the bainitic transformation was incomplete, resulting in a high level of martensite in the microstructures. As was mentioned, martensite is undesirable in these microstructures as it promotes a brittle behaviour.

Austempering Temperature (°C)	Cast sample thickness (mm)	Ultimate tensile strength (MPa)	Yield strength (MPa)	Total elongation (%)
280	12.5	1761	1640	2
	75	1715	1645	2
330	12.5	1330	1237	5
	75	1408	1309	3

Table 3: Ultimate tensile strength, yield strength and total elongation values for samples austempered at 280°C and 330°C for 360 minutes.

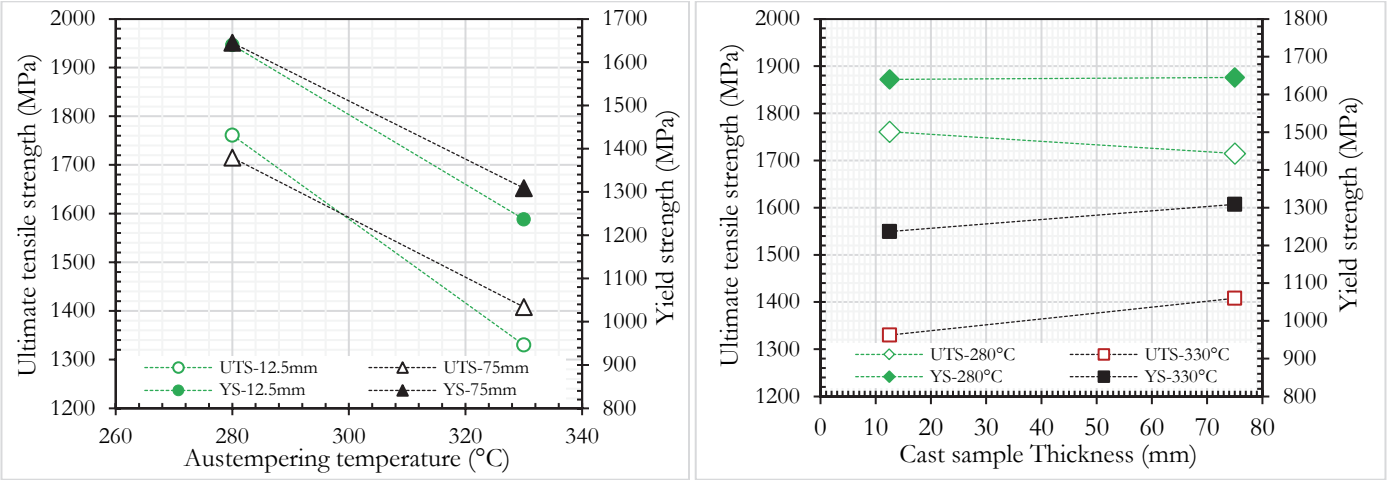

(a) (b)

Figure 7: Ultimate tensile strength and yield strength as a function of: (a) Austempering temperature, (b) Cast sample Thickness.

Discussion

The results show that microsegregation patterns significantly influence phase transformations during austempering heat treatments, affecting the type, morphology, and distribution of phases, particularly for transformation times shorter than those required to complete the bainitic transformation. This effect diminishes when the bainitic transformation is fully completed, leading to more homogeneous microstructures. This fact produces a low impact on the mechanical behaviour of these cast components when the solidification structure es evaluated.

The microstructures obtained at an austempering temperature of 280°C exhibited the highest UTS, approaching 1.7 GPa (Fig. 7a). These fine microstructures consist of nanometric bainitic ferrite plates and small blocks of retained austenite,

resulting in very low effective grain sizes. This microstructural refinement increases yield strength and hardness due to the presence of more barriers to dislocation movement, as explained by the Hall–Petch relationship[30].
Increasing the austempering temperature to 330°C led to lower tensile strength, yield stress, and hardness. Regarding total elongation, the steels treated at both austempering temperatures exhibited low ductility, which could lead to low toughness. This behaviour is attributed to the high carbon content of the steel, which increases the carbon level in retained austenite, reducing its deformation capacity. Additionally, casting defects such as non-metallic inclusions and shrinkage cavities further contribute to this reduced ductility.
No significant differences were observed in the mechanical properties between the two casting thicknesses studied (Fig. 7b). This is notable, as variations in solidification patterns would typically be expected to affect mechanical properties. These findings suggest potential advantages for using high-silicon steels with bainitic microstructures in cast components, particularly in industries like automotive, mining, and oil. Unlike in cast iron components, different casting thicknesses here exhibited similar mechanical properties, resulting in more uniform mechanical behaviour across the entire component, at least within the thickness range studied. However, this uniformity is unlikely for microstructures formed under shorter transformation times. In samples austempered at 230°C, the LTF regions showed smaller bainitic plates and a higher proportion of martensite formed during quenching. The presence of fresh (un-tempered) martensite contributes to a microstructure with poor ductility, leading to premature fracture. Other properties, such as fatigue limit or fracture toughness, may also degrade significantly under these conditions. This effect becomes more pronounced in smaller casting sizes, where microsegregation profiles are more distinct.
Therefore, to minimize heterogeneity in the mechanical properties of cast parts with different thicknesses, it is crucial to ensure that the bainitic transformation is fully completed to achieve a more uniform microstructure. This approach helps reduce the detrimental effects of microsegregation in these cast steel components.

CONCLUSIONS

A high-carbon, high-silicon steel casted into two different "Y" block thicknesses was subjected to austempering heat treatments to obtain carbide-free bainite. The main conclusions are summarized as follows:

- The difference between dendritic and interdendritic areas is more noticeable when the bainitic transformation is incomplete, which makes essential to achieve the transformation stop time to minimize the microstructural heterogeneity.
- Minimal differences in martensite start temperature, bainitic transformation time, phases fraction and mechanical properties were observed between different cast samples thicknesses. The most notable difference in the microstructures is the distribution of dendritic and interdendritic areas, which is coarser in the thicker casting.
- Different casting thicknesses exhibit comparable mechanical properties leading to enhanced uniformity in the mechanical behaviour of the entire component, which is remarkable.
- These results, combined with the relatively low cost of the bainitic High-Carbon and High-Silicon Cast Steel, may promote the applicability of high-silicon cast steels with bainitic microstructures in several industries, including the automotive, agricultural, and mining sectors.

REFERENCES

[1] Okuda, K., Ogawa, K., Ichikawa,Y., Shiozaki, T., Yamaguchi, N. (2019). Influence of microstructure on fatigue property of ultra high-strength steels, Frattura ed Integrità Strutturale, 48, pp. 125-134. DOI: 10.3221/IGF-ESIS.48.15.
[2] Lopez-Crespo, P., Withers, P.J., Yates, J. R., et al. (2013). Study of overload effects in bainitic steel by synchrotron X-ray diffraction. Frattura ed Integrità Strutturale, 25, pp. 153-160; DOI: 10.3221/IGF-ESIS.25.22.
[3] Toribio, J., Matos, J.C., González, B. (2017). Influence of crack micro-roughness on the plasticity-induced fatigue propagation in high strength steel, Frattura ed Integrità Strutturale, 41 pp. 62-65. DOI: 10.3221/IGF-ESIS.41.09.
[4] Zhao, F.Y., Chen, P., Xu, B., et al. (2020). A carbide-free bainitic steel with high-ductility by dynamic transformation during coiling process. Mater Sci Technol., 36(15), pp. 1704–1711. DOI: 10.1080/02670836.2020.1821966.
[5] Caballero, F.G., Roelofs, H., Hasler, S., et al. (2012). Influence of bainite morphology on impact toughness of continuously cooled cementite free bainitic steels. Mater Sci Technol., 28(1), pp. 95–102. DOI:10.1179/1743284710Y.0000000047.

[6] Garcia-Mateo, C. and Caballero, F.G. (2015). Understanding the mechanical properties of nanostructured bainite. In: Aliofkhazraei M. (ed) Handbook of mechanical nanostructuring. Weinheim: Wiley-VCH, pp. 35–65. DOI: 10.1002/9783527674947.ch3.
[7] Garcia-Mateo, C., Caballero, F.G. (2005). Ultra-high strength bainitic steels. ISIJ Int., 45(11), pp. 1736–1740.
[8] Morales-Rivas, L., Garcia-Mateo, C., Sourmail, T., et al. (2016). Ductility of nanostructured bainite. Metals, 6(12), pp. 302. http://hdl.handle.net/10261/3186.
[9] Garcia-Mateo, C., Paul, G., Somani, M.C., et al. (2017). Transferring nanoscale bainite concept to lower C contents: a perspective. Metals, 7(5), pp. 159. DOI: 10.3390/met7050159.
[10] Garcia-Mateo, C., Caballero, F.G., Sourmail, T., et al. (2012). Tensile behaviour of a nanocrystalline bainitic steel containing 3 wt% silicon. Mater Sci Eng A, 549, pp. 185–192. DOI: 10.1016/j.msea.2012.04.031.
[11] Peet, M.J., Hill, P., Rawson, M., et al. (2011). Fatigue of extremely fine bainite. Mater Sci Technol, 27(1), pp. 119–123. DOI: 10.1179/026708310X12688283410244.
[12] Das Bakshi, S., Leiro, A., Prakash, B., et al. (2014). Dry rolling/sliding wear of nanostructured bainite. Wear, 316, pp. 70–78. DOI: 10.1016/j.wear.2014.04.020.
[13] Lefevre, J., Hayrynen, K.L. (2013). Austempered materials for powertrain applications. J Mater Eng Perform, 22(7), pp. 1914–1922. DOI: 10.1007/s11665-013-0557-4.
[14] Žužek, B., Sedlaček, M., Podgornik, B. (2015). Effect of segregations on mechanical properties and crack propagation in spring steel. Frattura ed Integrità Strutturale, 34, pp. 160-168; DOI: 10.3221/IGF-ESIS.34.17.
[15] Tenaglia, N.E., Boeri, R.E., Basso, A.D., et al. (2016). Macro and microstructural characterisation of high Si cast steels – study of microsegregation patterns. Int J Cast Met Res, 30(2), pp. 103–111. DOI: 10.1080/13640461.2016.1258515.
[16] Tenaglia, N. E., Fernandino, D., & Basso, A. D. (2022). Effect of Ti addition and cast part size on solidification structure and mechanical properties of medium carbon, low alloy cast steel. Frattura Ed Integrità Strutturale, 16(62), pp. 212–224. DOI:10.3221/IGF-ESIS.62.15.
[17] Basso, A., Toda-Caraballo, I., San-Martín, D., et al. (2020). Influence of cast part size on macro- and microsegregation patterns in a high carbon high silicon steel. J Mater Res Technol, 9, pp. 3013–3025. DOI: 10.1016/j.jmrt.2020.01.052.
[18] Tenaglia, N.E., Massone, J., Boeri, R., et al. (2020). Effect of microsegregation on carbide-free bainitic transformation in a high-silicon cast steel. Mater Sci Technol., 36, pp. 690–698. DOI: 10.1080/02670836.2020.1732076.
[19] Basso, A.D., Toda-Caraballo, I., Eres-Castellanos, A., et al. (2020). Effect of the Microsegregation on Martensitic and Bainitic Reactions in a High Carbon-High Silicon Cast Steel. Metals, 10, 574. DOI: doi.org/10.3390/met10050574.
[20] Ennis, B., Jimenez-Melero, E., Mostert, R., et al. (2016). The role of aluminium in chemical and phase segregation in a TRIP-assisted dual phase steel. Acta Mater, 115, pp. 132–142. DOI: 10.1016/j.actamat.2016.05.046.
[21] Ahmed, M., Salam, I., Hashmi, F.H., et al. (1997). Influence of banded structure on the mechanical properties of a high-strength maraging steel. J Mater Eng Perform, 6, pp. 165–171. DOI: 10.1007/s11665-997-0009-0.
[22] Tenaglia, N.E., Boeri, R.E., Massone, J.M., et al. (2018). Assessment of the austemperability of high-silicon cast steels through Jominy hardenability tests. Mater Sci Technol, 34(16), pp. 1990-2000. DOI: 10.1080/02670836.2018.1507124.
[23] Yang, H.S., Bhadeshia, H.K.D.H. (2006). Uncertainties in dilatometric determination of martensite start temperature. Mater Sci Technol, 23, pp. 556–560. DOI: 10.1179/174328407X176857.
[24] Sourmail, T., Garcia-Mateo, C. (2005). Critical assessment of models for predicting the Ms temperature of steels. Comput Mater Sci, 34, pp. 323–334. DOI: 10.1016/j.commatsci.2005.01.002.
[25] Bhadeshia, H.K.D.H. (2001). Bainite in Steels: Transformations, Microstructure and Properties. 2nd ed. London: IOM Communications Ltd, pp. 122–128.
[26] Bhadeshia, H.K.D.H. (1981). Bainite: The Incomplete-Reaction phenomenon and the approach to equilibrium. International Solid-Solid Phase Transformations Conference (ed IA Hubert), Pittsburgh, PA, USA, 10–14 August.
[27] Caballero, F.G., Santofimia, M.J., García-Mateo, C., et al. (2004). Time-Temperature-Transformation Diagram within the Bainitic Temperature Range in a Medium Carbon Steel. Mater Trans, 45, pp. 3272–3281. DOI: 10.2320/matertrans.45.3272.
[28] Santajuana, M.A., Eres-Castellanos, A., Ruiz-Jimenez, V., et al. (2019). Quantitative Assessment of the Time to End Bainitic Transformation. Metals, 9, pp. 925. DOI: doi.org/10.3390/met9090925.
[29] Shelar, A. & Ronge, B.P. (2023). Characterization of mechanical properties and microstructural evolution of martensitic steel in repeated tempering cycles. Fracture & Structural Integrity, 66, pp. 38-55. DOI: 10.3221/IGF-ESIS.66.03
[30] Hall, E.O. (1954). Variation of Hardness of Metals with Grain Size. Nature, 173, pp. 948–949. DOI: doi.org/10.1038/173948b0.